AD NUMBER

ADB014175

NEW LIMITATION CHANGE

TO

Approved for public release, distribution unlimited

FROM

Distribution authorized to U.S. Gov't. agencies only; Test and Evaluation; SEP 1976. Other requests shall be referred to Army Ballistic Research Labs., Aberdeen Proving Ground, MD 21005.

AUTHORITY

USAARDC ltr 8 Mar 1978

BRL

AD

MEMORANDUM REPORT NO. 2686

INVESTIGATIONS OF TRANSITIONAL BALLISTICS IN MUZZLE JET FLOW SIMULATORS

Fritz H. Oertel, Jr.

September 1976

USA BALLISTIC RESEARCH LABORATORIES
ABERDEEN PROVING GROUND, MARYLAND

Destroy this report when it is no longer needed.
Do not return it to the originator.

Secondary distribution of this report by originating or sponsoring activity is prohibited.

Additional copies of this report may be obtained from the Defense Documentation Center, Cameron Station, Alexandria, Virginia 22314.

The findings in this report are not to be construed as an official Department of the Army position, unless so designated by other authorized documents.

UNCLASSIFIED

SECURITY CLASSIFICATION OF THIS PAGE (When Data Entered)

REPORT DOCUMENTATION PAGE

READ INSTRUCTIONS BEFORE COMPLETING FORM

1. REPORT NUMBER — AMR — BRL ~~Memorandum Report No.~~ 2686

2. GOVT ACCESSION NO.

3. RECIPIENT'S CATALOG NUMBER

4. TITLE (and Subtitle)

INVESTIGATIONS OF TRANSITIONAL BALLISTICS IN MUZZLE JET FLOW SIMULATORS.

5. TYPE OF REPORT & PERIOD COVERED

Final

6. PERFORMING ORG. REPORT NUMBER

7. AUTHOR(s)

Fritz H. Oertel, Jr

8. CONTRACT OR GRANT NUMBER(s)

9. PERFORMING ORGANIZATION NAME AND ADDRESS

USA Ballistic Research Laboratories
Aberdeen Proving Ground, Maryland 21005

10. PROGRAM ELEMENT, PROJECT, TASK AREA & WORK UNIT NUMBERS

RDT&E 1T161102A33H

11. CONTROLLING OFFICE NAME AND ADDRESS

U.S. Army Materiel Development & Readiness Command
5001 Eisenhower Avenue
Alexandria, Virginia 22333

12. REPORT DATE

SEPTEMBER 1976

13. NUMBER OF PAGES

38 (12) 35 p.

14. MONITORING AGENCY NAME & ADDRESS (If different from Controlling Office)

15. SECURITY CLASS (of this report)

UNCLASSIFIED

15a. DECLASSIFICATION/DOWNGRADING SCHEDULE

16. DISTRIBUTION STATEMENT (of this Report)

Distribution limited to US Government agencies only; Test and Evaluation; Sep 1976. Other requests for this document must be referred to Director, USA Ballistic Research Laboratories, ATTN: DRXBR-TS, Aberdeen Proving Ground, MD 21005.

17. DISTRIBUTION STATEMENT (of the abstract entered in Block 20, if different from Report)

DDC RETURNED

18. SUPPLEMENTARY NOTES

19. KEY WORDS (Continue on reverse side if necessary and identify by block number)

Transitional (Intermediate) Ballistics
Muzzle Jets
Blast Simulation
Unsteady Expansion
Supersonic Underexpanded Jet
Laser Q-Switch
Sequential Laser Interferograms
Shadowgrams
Pitot Pressure
Static Pressure
Shock Position
Inner or Recompression Shock
Outer Shock

20. ABSTRACT (Continue on reverse side if necessary and identify by block number)

Two muzzle jet flow simulators which use clean propelling gases of known properties are described. Photographs and pressure data obtained in the simulators as a jet forms behind a shock wave which has left the simulator muzzle are shown and discussed. Of particular interest is an experiment using a ruby laser as a multiple-pulse light source to obtain a sequence of several laser interferograms for a single run from which quantitative data can be obtained. It was shown that the growth of the outer shock wave obeys → next page

DD FORM 1 JAN 73 1473 EDITION OF 1 NOV 65 IS OBSOLETE

UNCLASSIFIED

SECURITY CLASSIFICATION OF THIS PAGE (When Data Entered)

C5075

R_s is approximately a power law in time; the exponent ~~is n a~~ 0.715. Scaling of the inner shock wave development is also discussed. Inner and outer shock wave motion appeared to be coupled in the quasi-steady flow regime.

Spark shadow photographs of jet formation after a projectile uncorks the muzzle are also shown and discussed--optical probing of the real environment near the muzzle of guns is virtually impossible.

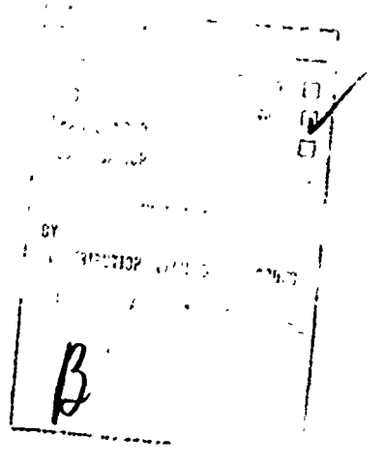

TABLE OF CONTENTS

LIST OF ILLUSTRATIONS

LIST OF ILLUSTRATIONS (Continued)

I. INTRODUCTION

When a tube-launched projectile uncorks the muzzle, high pressure propelling gases expand to a velocity which is much faster than the projectile velocity. The expansion, at first unsteady, with gasdynamic properties in the expanding muzzle jet flow changing quickly with time, becomes quasi-steady as conditions in the jet change more slowly with time.

Early theoretical and experimental studies were made of the quasi-steady flow regime[1*,2]. Using spark shadow photography of bullets being fired from small caliber weapons, it was shown that the expansion of propellant gases for supersonic firings is characterized by the formation of an underexpanded jet structure having embedded shocks and a mixed supersonic/subsonic flow. More recent experiments[3,4] examined the quasi-steady flow ahead of guns in greater detail. Additionally, in connection with propulsion, control, and guidance of aerospace systems, many theoretical and experimental studies have been made of the steady, underexpanded jet. References 5 and 6 survey much of the work done for

---

1. *K. Oswatitsch, "Intermediate Ballistics," Deutsche Luft und Raumfahrt Forschungs - Bericht 64-37, DVL Bericht 358, 1964.*

2. *C. Cranz and B. Glatzel, "Die Ausströmung von Gasen Bei Hohen Anfangsdrucken," Ann. der Physik, Vol. 43, 1914.*

3. *G. A. Schroeder, "Experimentelle Untersuchungen zur Stroemungsausbildung in der Pulvergasglocke," Bericht E4-71, Arbeitsgruppe für Ballistische Forschung, Weil am Rhein, 1971.*

4. *E. M. Schmidt and D. D. Shear, "The Formation and Decay of Impulsive, Supersonic Jets," AIAA Paper No. 74-531, AIAA 7th Fluid and Plasma Dynamics Conference, Palo Alto, CA, June 1974. Also BRL Report 1692, "The Flow Field About an M-16 Rifle," January 1974, AD 916646L.*

5. *E. M. Schmidt, "Muzzle Devices, A State-of-the-Art Survey. Volume I: Hardware Study," BRL Memo Report 2276, February 1973, AD 909325L*

6. *T. C. Adamson, Jr., "The Structure of the Rocket Exhaust Plume Without Reaction at Various Altitudes," Supersonic Flow, Chemical Processes and Radiation Transfer, Pergamon Press, New York, 1964.*

**This is part of an area of ballistics called intermediate ballistics by Oswatitsch[1]. We call it transitional ballistics, defined as the coupling of the projectile's interior ballistics phase with its free flight aerodynamic phase. It deals with interactions between the projectile and its tube launcher at exit from the muzzle, interactions between the projectile and muzzle effluents, and coupling of the tube emptying process to the flow field at the muzzle.*

steady and quasi-steady jets. Only a small number of papers have been devoted to the unsteady, underexpanded jet and they have been limited to free jets issuing from very small orifices, for example, references 7 and 8.

Making measurements near the muzzle of guns is difficult. This difficulty, caused primarily by particulate matter in the muzzle effluents which can damage probes and can make the gas opaque to optical probing, has limited previous studies to the quasi-steady flow far from the muzzle where the gases are more transparent. However, we are interested in the unsteady flow very near the muzzle of guns where muzzle devices operate and where the most significant gasdynamic forces and moments can be imparted to a projectile during its transitional ballistics phase. We want to be able to "see" the development of the unsteady flow field soon after a projectile emerges from the muzzle and we want to make measurements in it for eventual comparison with several competing hydrodynamic computer codes[9].

To overcome these experimental problems and to have laboratory control over operating conditions, muzzle jet flow simulators were constructed, each with its own characteristics and advantages, which use clean propelling gases of known properties. In these simulators, we have made photographs of the fundamental case of an unsteady flow field free of a projectile's disturbance; that is, of the axisymmetric, supersonic, underexpanded jet which forms behind a normal shock wave after it leaves the tube. For this case, we have also made pressure and heat transfer measurements at the muzzle and in the expanding flow field ahead of the muzzle on the jet axis. We have also made photographs of the developing flow field soon after a projectile leaves the muzzle. Of particular interest is an optical technique using a ruby laser as a multiple-pulse light source which we have found useful to obtain a sequence of several laser interferograms for a single simulator run[10]. One big advantage of this technique is that in the clean gas

---

7. *J. D. Buckmaster, "An Investigation of Cylindrical Starting Flows," AIAA Journal, Vol. 2, No. 8, September 1964.*

8. *I. M. Naboko, T. V. Bazhenova, A. I. Opera, and V. A. Belavin, "Formation of a Jet of Shock-Heated Gas Outflowing into Evacuated Space," Astronautica Acta, Vol. 17, Pergamon Press, New York, 1972.*

9. *C. K. Zoltani, "Evaluation of the Computer Codes BLAST DORF, HELP, and HEMP for Suitability of Underexpanded Jet Flow Calculation," BRL Report 1659, August 1973, AD 768708.*

10. *F. H. Oertel, Jr., "Laser Interferometry of Unsteady, Underexpanded Jets," Proc. Int'l. Cong. Instr. in Aerospace Simulation Facilities, California Institute of Technology, Pasadena, CA, 1973. Also BRL Report 1694, January 1974. AD 773664.*

of the simulator, it is possible to obtain quantitative data for the entire flow field (contours of constant density) at several instants in time during the unsteady flow development near the muzzle and in the later quasi-steady flow. Since all the photographs are obtained for one run, the interpretation of data is not complicated by initial conditions differing from run-to-run.

The above experiments and the muzzle jet flow simulators in which they were done will be discussed in this paper.

II. SIMULATORS

Figures 1 and 2 show dimensions and details of the two muzzle jet flow simulators we have used, which shall be called MJS-1 and MJS-2, respectively. In each facility, clean, high pressure gases of known properties rupture a diaphragm and drive a projectile down the tube to exit into the test section containing a receiver gas. Or, when there is no projectile in the tube, a shock wave propagates into the receiver gas after the diaphragm ruptures. In both simulators, we can use a variety of gases as the driver and receiver gases. In this way, we can vary experimental parameters, such as ratio of specific heats, molecular weight, Mach number, propellant energy, projectile and shock velocities, etc.

The simulator shown in Figure 1, MJS-1, resulted from modification of a shock tube. Conversion to a muzzle jet flow simulator was accomplished by bolting a mounting or breech plate to the shock tube's test section. A tube with a 25.4mm diameter smoothbore was screwed into the plate. The result was a "gun" with an essentially infinite chamber length. We used a scribed aluminum diaphragm ($\sim$ 0.8mm thick with an unsupported area of 25.4mm diameter) to seal the tube.

In this simulator, the high pressure reservoir of propelling gases was created by shock reflection in the following way. Using combustion-heating of helium[11], the pressure in the shock tube's driver (located upstream to the left on Figure 1) was increased so that the diaphragm between the driver and driven sections ruptured. The resulting shock wave propagated down the shock tube to be reflected from the breech plate, thereby increasing the temperature and pressure of the air there. For these experiments, the shock tube driven section contained air at 0.41 atm; the stagnated air pressure and temperature were in the neighborhood of 70 atm and 2000°K, respectively.

---

11. *I. I. Glass and J. G. Hall, Handbook of Supersonic Aerodynamics, Shock Tubes, Section 18, NAVORD Report 1488 (Vol. 6), 1959.*

MJS-2 was fabricated from a 37mm gun smoothbored to a diameter of ∿ 38mm. It has a spin-on breech and a diaphragm holder which is loaded like a cartridge. We used unscribed aluminum diaphragms (∿ 1mm thick with an unsupported area of ∿ 12.7mm) to separate the driver gas from the receiver gas. Diaphragm opening pressure was ∿ 270 atm. With a projectile ahead of the diaphragm, the simulator is a gun. Without a projectile, it is a conventional shock tube. We operated with cold helium, cold nitrogen, and combustion-heated helium drivers; the receiver gas was air.

MJS-1 is quite large: it requires at least two men to safely prepare it for a run. MJS-2 can be prepared easily by one man in a short time. Because of the short time needed to prepare MJS-2 for a run, it was used for most of our testing.

The main advantage of MJS-1 over MJS-2 is that the flow behind a projectile launched using air or nitrogen is laminar. This is essential for interferometry, because the disordered nature of turbulent flow destroys the fringe pattern. Interferograms made of the flow from MJS-1 with air as the propelling gas and air as the receiver gas showed no turbulence. The Reynolds number for this flow was well below the critical Reynolds number for transition from laminar to turbulent flow[11,12]. For a projectile launched from MJS-2, the Reynolds number for heavy gases such as air and nitrogen was near the critical Reynolds number. Since the MJS-2 tube is much longer than the MJS-1 tube, the flow has more time to transist. Also, the reservoir in MJS-1 may have smaller initial disturbances than the reservoir in MJS-2. Even for shock waves propagating into air in MJS-2, a transition to turbulence was seen late in the flow, but only after we were no longer interested in the jet development. For a light gas (helium) driver, there was no noticeable turbulence of the gas behind projectiles launched from MJS-2.

III. EXPERIMENT

A. Optical Techniques

The optical set-up for our experiments using sequence laser interferometry is shown in Figure 3. Major components are the laser light source, Mach-Zehnder optical interferometer, and high speed camera. The flow direction shown is for MJS-1; flow is in the opposite direction for MJS-2, but, for clarity, they are shown to be the same in this report.

1. Sequence Laser Light Source

To photograph the transient processes occurring at the muzzle

---

12. *H. Schlichting, Boundary Layer Theory, McGraw-Hill Book Company, Inc., New York, 1960.*

of our simulators, we developed a multiple-pulse light source. We tried electro-optic (Pockels cell) and passive (bleachable dye absorber) Q-switching a ruby laser. The latter proved to be more reliable[10].

Passive Q-switching is accomplished by placing a cell containing a reversible, bleachable dye solution between the laser head and the 100% reflector, as in Figure 3. Cryptocyanine dissolved in methanol has the proper absorption characteristics for the ruby laser's fundamental wavelength of 6943Å. The metal ion occupying the center of the complex molecule in solution affects the exact location of the absorption band peaks and the relaxation rates (rates for the ion to return to its normal absorbent condition). The concentration of the dye and the length of the cell (∿ 1 cm) are so arranged that cell transmission is approximately 50% when the photon density from the rod is low. As pumping continues, the photon density rises rapidly, saturating the available ionic energy levels and the dye bleaches. Cavity gain increases rapidly and a giant pulse is generated with a typical pulse width of 10-20 ns, often much shorter than those generated by electronic shutters, a difference which can be critical for our experiments.

Control of jitter (uncertainty in the time giant pulsing occurs) is also important for these experiments. In practice, we have found that for careful control of the dye concentration and pumping voltage, a jitter of less than ± 10 μs was common for both the single-pulse and multiple-pulse modes--somewhat better than the specification of ± 50 μs quoted by most manufacturers. To a lesser extent, the number of pulses and their separation could also be regulated by careful attention to these variables.

2. Cameras

Two cameras were used in these experiments: a single frame camera for the shadowgrams, and a multi-frame, high speed camera for the finite fringe interferograms. The shadow camera used was typical of many such cameras which use parallel light to illuminate the shadow field and a second lens (L_3 on Figure 3) for image formation. A nanosecond duration (∿ 40 ns) spark light source with a diameter of ∿ 0.5mm was used to backlight the flow field.

To make the interferograms, the Mach-Zehnder optical interferometer, which operates on the principle of ray amplitude division[13], was backlighted by the sequence laser light source, as shown on Figure 3. In the film plane one sees, for each laser pulse, a pattern

---

13. R. L. Rowe, "Interferometers for Hypervelocity Ranges," ISA Trans., Vol 5, No. 1, 1966.

of alternate light and dark fringes which are parallel in the undisturbed gas, but shift in the disturbance.

The high speed camera on Figure 3 is slitless and shutterless. It consists of lens, L_3, and a rotating 4-sided mirror which sweeps images of the laser-illuminated event onto a stationary strip of film $\sim$ 240mm wide x 3m long. The film drum is located $\sim$ 1.04m from the front surface of the rotating mirror for a test area magnification of $\sim$ 0.88. Commercial high speed panchromatic film (ASA 1250) with an extended red sensitivity was used to record the interferograms (and shadowgrams).

The mirror is rotated by a cone-shaped turbine driven by bottle gases. The turbine is unique in that the driving gas also serves as a fluid bearing. For some experiments, we used nitrogen at an inlet pressure of $\sim$ 4 atm to drive the mirror at $\sim$ 75,000 RPM--a writing speed of 16.2mm/μs or, for our optics, a framing rate of $\sim$ 100,000 frames/s.

3. Typical Optical Experiments

First we will describe a typical sequence laser experiment done in MJS-1 after a normal shock leaves the tube. There are several events to be synchronized over which we have little control; such as: the mirror is spun-up to full speed at the time of the experiment so its orientation cannot be controlled; the film drum is not a full 180° arc so photographs can be lost; and the dye-controlled shutter cannot be triggered precisely (as an electronic shutter can). In addition, when using a laser as a light source for photography, 500-1000 μs must be allowed for pumping the laser rod--irrespective of the method of Q-switching.

For a completely synchronized experiment, the shock should exit from the tube as the first laser pulse is generated; and subsequent laser pulses should be of equal intensity with precisely-set spacing between pulses. Moreover, the rotating mirror should be oriented so that all pulses will be reflected onto the film.

We found that we could predict onset of lasing much more accurately than we could predict shock exit. Therefore, we found it best to first adjust for several laser pulses, then to set timing so that the expected time of shock exit would be bracketed by the pulse train. For this experiment, duration of the pulse train could not be more than $\sim$ 185 μs (the time for the mirror to complete a sweep of the film) or a portion of the film might be doubly-exposed. To prevent this rerun, duration of the pulse train was tailored by readjusting the dye concentration or pumping voltage, but care had to be taken not to lose the other pulse train characteristics we wanted.

Figure 4 shows an oscilloscope trace of the static pressure measured in MJS-1 by an electrically-isolated, calibrated piezoelectric pressure gage shock-mounted in the wall of the tube 3.97mm from the exit plane. (A second pressure gage was mounted about midway between

the diaphragm and the muzzle to serve as a trigger for peripheral equipment and so that shock velocity could be measured.) Passage of the shock is indicated by an abrupt increase in amplitude. Pressure remains constant as the shock-heated air flows past, followed by the cooler air behind the contact front. The pressure is seen to increase after ∿ 40 μs as upstream disturbances arrive. The sequence of laser pulses for this run is also shown on the trace. The shape of each laser pulse is due to saturation of the photoelectric diode (solar cell) used to record the pulses. The laser interferograms made for the first three pulses on Figure 4 are reproduced in Figure 5; elapsed times after the shock wave leaves the tube are given under each photograph, and conditions at exit are given in the caption. A sequence of laser photographs made similarly in MJS-2 for a nitrogen driver are shown in Figure 6, where particulars are again in the caption.

Using the nanosecond-duration spark light source and camera described earlier, shadow photographs were made for separate runs at various times after normal shock waves and projectiles left the 38mm tube of MJS-2 to enter the test section containing air at a pressure of ∿ 0.041 atm. Two series of spark shadow photographs are shown in Figures 7 and 8. The elapsed times after exit from the tube are shown below each frame and conditions measured at exit are given in the captions. The flow of nitrogen propelling gas is clearly turbulent, as discussed in the section on simulators.

Before leaving this section, it is worth mentioning that duration of the light pulses is very important for these highly transient gasdynamic processes. For example, if the pulse duration is ∿ 2 μs, as for a BH-6 mercury arc source commonly used for interferometry or for a crowbarred spark light source, a shock wave moving at a velocity of 2000 m/s will move 4mm on a fixed piece of film (shadow photograph) during the exposure time, too much for resolution of the shock wave. For our nanolite and for the laser, the exposure times were ∿ 1/50 that of such a source, so that shock movement was only a fraction of a millimeter. This problem of pulse duration is even more critical for swept image photography using the rotating mirror. At a mirror rotational speed of ∿ 80,000 RPM, the writing speed on the film is ∿ 17mm/μs. For a pulse width of 30 ns, the image will be smeared for ∿ 1/2mm, which we have found to be satisfactory for resolution of the interference fringe pattern. We have noticed pulses of this duration and shorter for our ruby rod of select optical quality. For ordinary rods, duration of pulses is much longer. Photographs made with pulses from these rods exhibited objectionable streaking of the grain pattern at the mirror rotational speed used.

B. Other Instrumentation Techniques

Both simulators were instrumented so that pressure, velocity, and heat transfer measurements could be made. Only a few heat transfer measurements were made using a thin-film gage[11]. For each run, static

pressure-history and velocity were measured at two locations in the tube as described earlier in connection with Figure 4.

For the nonprojectile runs in MJS-2, shock waves propagated into air at a pressure of $\sim$ 0.041 atm at velocities of $\sim$ 1900 m/s (helium driver) and $\sim$ 1000 m/s (nitrogen driver). For both drivers, the diaphragm bursting pressure was $\sim$ 270 atm and the driver gas temperature was in the neighborhood of 300°K. These were also the driver conditions when projectiles were launched, except for the combustion-heated helium driver where pressures were the same, but temperatures were an order of magnitude higher.

For shock wave runs in MJS-2, pitot pressure and static pressure were measured on the axis of the tube at several locations downstream of the muzzle. Static pressure measurements were made with the pancake gage[14] shown in the insert on Figure 9a, a spark shadow photograph showing the gage sting-mounted in the flow. The pancake portion of the gage is 24.3mm in diameter and is 1.8mm thick. The piezoelectric sensing element, located in the center of the pancake, is exposed to the flow on its upper and lower surfaces. Pitot pressure was measured with the gage shown similarly in Figure 9b. The piezoelectric sensing element is $\sim$ 5.6mm in diameter. Care was taken to compensate for thermal and acceleration effects and to reduce cable noise.

Figures 10 and 11, respectively, show sample oscilloscope traces of static pressure and pitot pressure for different runs after a shock wave leaves the tube at a velocity of $\sim$ 1900 m/s, the same flow conditions as for the shadow photographs, Figure 7. For the top trace in each figure, the gage is closer to the muzzle than for the bottom trace, as shown in each caption. Several such traces were made for other gage locations, and shadowgrams such as those in Figure 9 were made. For each run, the angle between the axis of sting-mounted gage and the axis of the tube was two degrees or less.

IV. RESULTS AND DISCUSSION

A. Optical Data

The interferograms shown in Figures 5 and 6 can be reduced to a series of maps of constant density contours--one map for each photo-

---

14. *P. S. Westine and F. Hoese, "Blast Gauge for Measuring Shocks with Short Wavelengths," Southwest Research Institute Interim Report, Contract No. 0178-69-C-0318, May 1970.*

graph--by methods described, for example, in references 15 and 16. Reduction is to begin soon using an automatic fringe reader.

Figures 5 and 6 are qualitatively similar. In both figures, the shock wave expanding from the muzzle (outer shock) is indicated by a sharp upward fringeshift caused by a density increase through the shock as one moves from the straight, parallel fringe pattern of the undisturbed receiver gas into the disturbance. Within the disturbance, Figure 5c and Figures 6e and 6f, there is a rather sharp increase in the fringeshift as one moves from the tube in the flow direction. This is caused by the density jump through the recompression shock or inner shock (Mach disc for steady, underexpanded jets) which recompresses the rapidly-expanded tube gas to match pressure with the gas behind the outer shock. At earlier times there is also an indication of a shock, resulting from expansion of the tube gas at the lip of the tube, which grows to become the completed inner shock. One should be careful when interpreting axisymmetric interferograms, because fringeshift depends on geometry as well as density, but these discontinuities are clear.

The shock waves in the vicinity of the lip are seen more clearly on the shadow photographs of Figure 7; an intercepting shock and jet boundary are also seen. The intercepting shock is formed when expansion waves from the muzzle reflect from the jet boundary as compression waves which coalesce to become the intercepting shock. A contact front is seen between the shock waves. It is an entropy discontinuity between the tube gas and the gas behind the expanding outer shock wave. The inner and outer shock wave motion is reproduced as a function of time on Figure 12 from photographs like those in Figure 7 made for runs in MJS-2 for which the measured in-tube shock velocity was repeatable to within ± 2%, much better than in MJS-1 and better than in either simulator when launching projectiles.

It is seen on Figure 7a that the recompression shock, intercepting shock, and contact front are formed almost instantaneously due to lateral expansion of the tube gas at the lip of the tube. At these

---

15. *R. Ladenburg, C. C. Van Voorhis, and J. Winckler, "Interferometric Studies of Faster than Sound Phenomena, Part II. Analysis of Supersonic Air Jets," Phys. Rev., Vol. 76, No. 5, 1949.*

16. *F. D. Bennett, W. C. Carter, and V. E. Bergdolt, "Interferometric Analysis of Air Flow About Projectiles in Free Flight," J. Appl. Phys., Vol. 23, No. 4, 1952; also BRL Report No. 797, March 1952, AD 801758.*

early times, the gas on the axis does not feel the lack of lateral constraints. This is implied by the still-normal shock wave on the axis in Figures 7a and 7b. On other photographs, we observed that in the neighborhood of 23 μs, the apparent center of the outer shock expansion appeared to literally jump from the face of the muzzle to a point on Figure 7c ∿ 13mm ahead of the muzzle. (Soon thereafter, it increased linearly with time.) Before 23 μs, the apparent center was inside the tube. At those early times, assigning a location to the expansion center is nebulous, but a jump is still evident. On these photographs and others (Figures 5a and 6c and d), we have seen a bulge of the outer shock in the axial direction near the jet axis. This bulge persists for more than 20 μs for the conditions of Figure 7 until the outer shock takes on a more spherical shape as the inner shock begins to form on the axis of the jet. Between Figures 7d and 7e, the incomplete inner shock first conforms to the shape of the outer shock (the hint of a sharp gradient due to the inner shock is seen in the vicinity of the jet axis on Figure 7e), then the gradients increase in strength and formation is complete ∿ 10 μs after Figure 7d. On Figure 12 we see that the inner shock wave grows steadily without changing shape appreciably (as does the intercepting shock) until it closes quickly to the jet axis. (Some contours which make the progress of this closure clearer were omitted, because they were too close together.) The interface between the shocks does not appear to close to the axis and adjust as quickly. It is still deformed on Figure 7f. Once the inner shock wave is formed, the flow appears to be quasi-steady and the inner and outer shocks propagate together, appearing to be scaled replicas of one another, as observed in reference 7 for expansion of a two-dimensional supersonic jet from a small orifice.

For the projectile runs, Figure 8, certain features of the flow-field are qualitatively similar to the free jet runs. Others are clearly different because of the projectile's influence. First, as the projectile uncorks the muzzle, a small annular orifice is formed. A choked condition exists for an instant so that the propelling gases expand supersonically into the receiver gas from an initially sonic condition. This outer shock is seen to be affected by the presence of the projectile. For this small orifice, the inner shock and intercepting shock are formed "instantaneously." After formation, the inner shock is qualitatively the same as for non-projectile runs; only the turning angle of the flow is larger, because the ratio of exit pressure to ambient pressure, p_e/p_∞, is larger here. For these projectile runs, the flow of propelling gases is turbulent, as discussed earlier, so the interface between the ambient air, which has been processed by the outer shock wave, and the propelling gases cannot be located precisely.

The most striking influence of the projectile is the shock wave at the projectile base which moves with the projectile velocity (to experimental accuracy). We noted that it is not until later in the expansion that the shock wave at the base takes on the characteristics

of a true "bow" wave; that is, the extremities of the shock bend in the flow direction. When that happens, the location of the extremities relative to the inner shock is nearly the same as we see in these photographs.

B. Flow Characteristics in the Simulators

Shock tube flow from the muzzle has similar characteristics in both simulators. For example, since the flow behind the normal shock waves was always supersonic, pressure relief at the muzzle was not felt upstream in the tube. As a consequence, the pressure at the muzzle remained constant after an abrupt increase as the shock passed--for $\sim$ 40 μs (Figure 4) in MJS-1 and in MJS-2 for $\sim$ 200 μs for the fast shock wave and $\sim$ 400 μs for the slow shock wave. However, although pressure (and velocity) remain constant during this time, the Mach number--hence, the energy flux from the tube[17] --increases abruptly as an in-tube contact front passes. This contact front is an interface between the cool driver gas and the shock-heated tube gas.

Preliminary measurements in MJS-2 with thin-film heat transfer gages sting-mounted on the tube axis near the muzzle and in the tube wall near the muzzle showed a jump as the shock wave passed, then a linear voltage response by the gage. The traces imply that the flow behind the shock wave has constant properties which last $\sim$ 140 μs for the fast shock wave and $\sim$ 370 μs for the slow shock wave. These times are in good agreement with the theoretical "useful test times" computed for real air from Figures 5.1-4a and -4b of reference 11 and halved, as recommended by the authors to bring theoretical test times into agreement with times observed by others. The test time predicted in this way for the run of Figures 4-6 was $\sim$ 30 μs. The traces indicated that for the slow shock wave, where the driver gas was nitrogen, the test time was ended by the flow becoming turbulent. Turbulence was also seen on late-time interferograms for this driver gas after we were no longer interested in jet development.

The pitot pressure traces in Figure 11 for the fast shock wave show that for the gage nearest the muzzle, the total pressure remained constant for nearly 100 μs after the outer shock wave passed. (The static pressure at the muzzle for this flow remained constant for $\sim$ 200 μs.) This time is comparable to the theoretical and experimental times mentioned in the previous paragraph, which measure when the contact surface leaves the tube. Most of our pictures were made for this fast shock before 100 μs had elapsed.

---

17. *A. K. Celmins, "Theoretical Basis of the Recoilless Rifle Interior Ballistics Code RECRIF," BRL Report (to be published).*

At the farthest gage location, there is a distinct plateau behind the shock wave. This plateau was correlated to the region between the outer and inner shock waves using Figure 12 and the shadow photographs of gage location, such as in Figure 9. All traces made with the gage located beyond the point where the inner shock wave closed to the jet axis showed this plateau. The decrease in pitot pressure following the plateau was associated with flow of the underexpanded gases over the gage. Notice that for the static pressure, Figure 10, the pressure in the core during early jet development (top trace) was quite high, but it clearly showed underexpansion in the lower trace as the gage pressure fell below ambient receiver pressure. The change in slope of the decreasing pressure appears to take place at about the same time for all traces made after the inner shock wave is complete; it lags the pressure rise in the outer shock wave by $\sim$ 20 μs. This constant lag, which could be associated with what appears to be self-similar growth of the two shocks, was also seen when the inner and outer shock positions, Figure 12, were overlaid on the gage locations, such as Figure 9.

Figure 13 shows peak static pressure and peak pitot pressure measured just behind the outer shock wave plotted as a function of time. The times correspond to those on Figure 12. They are delay times from the gage which triggers the oscilloscopes and the spark light source. Using them here makes it easier to compare pressures and optical data. The pressures were normalized by dividing by standard atmospheric pressure.

For projectile launches, the muzzle pressure ratio, p_e/p_∞, for a heavy gas driver (air or nitrogen) is higher in MJS-1 ($\sim$ 350 - 500) than in MJS-2 ($\sim$ 150 - 250) for projectile muzzle velocities in the subsonic to low supersonic range, although the reservoir pressure was about a factor of four higher in MJS-2. This was true, because of the larger volume of the longer and larger MJS-2 tube.

C. Scaling

The time for the inner shock wave to form on the jet axis should scale with the time it takes for a signal to propagate across the muzzle at the local sound speed at the muzzle. That says that if it takes 60 μs for the inner shock to form for the fast shock wave in MJS-2, it should take $\sim$ 100 μs for the inner shock to form behind the slow shock wave. This is borne out by the photographs like Figure 6. For the run in MJS-1, this time should be less than in MJS-2 by the ratio of tube diameters and less by the ratio of sound speeds behind the respective shock waves; that is, $\sim$ 35 μs. This is the time observed for the inner shock to form in this case. These results are apparently independent of pressure ratio at the muzzle which is quite different for each case.

Axial distances from the muzzle to the outer shock, X_o, to the inner shock, X_i, and to the apparent center, X_c, of the radially-expanding outer shock (inner shock and outer shock are closely concentric shortly after the inner shock formation is complete) were measured from interferograms and shadowgrams for several runs. These measurements are shown plotted on Figure 14 as functions of elapsed time after leaving the muzzle. Data points for the outer shock wave at very early times--when the apparent center was negative--were not plotted. The flagged symbols on the figure denote runs made in MJS-2; the plane symbols are for runs made in MJS-1. All measurements were made from sequence interferograms, except the X's, which were made from the series of shadowgrams, such as in Figure 7. Shock position is normalized by dividing by the diameter of the tube in MJS-1.

The data for the outer shock wave in MJS-1 show that its growth obeys a power law $X_o - X_c \sim t^n$, where $n = 0.715$. This value for the exponent agrees well with results for the case of a supersonic jet of air pushed from the barrel of a rifle ahead of a bullet traveling at supersonic speed $(n = 0.767)$[4]. That flow is similar to the flow in MJS-1 in that the energy flux increases step-wise during the testing time as the in-tube contact surface passes[17]. Theory for a spherical blast wave (see, for example, reference 18) shows that $n = 3/5$ for a constant rate of energy addition; when the rate of energy addition is linear in time, the exponent is $n = 4/5$. These two theoretical values bracket the experimental values above.

Since the energy flux from MJS-2 should be constant during the testing time, we would expect $n = 0.6$. A straight line with this slope is shown faired through the data points measured from the shadow photographs in MJS-2 for the fast shock. Agreement is satisfactory, but for the points beyond $\sim$ 30 μs, a slope of 0.715 would fit as well. The data measured from interferograms (where scatter of the data is smaller) made for fast and slow shock runs in MJS-2 indicate that the exponent should be ~ 0.715. So, for all runs in both simulators, the power law describing the outer shock wave's growth has the same exponent. Only the proportionality constant is different, because the initial conditions are different for each run.

The inner shock motion also appears to obey a power law variation, but its behavior is not as predictable as that of the outer shock.

---

18. *J. I. Erdos and P. D. Del Guidice, "Gas Dynamics of Muzzle Blast," AIAA Paper No. 74-532, AIAA 7th Fluid and Plasma Dynamics Conference, Palo Alto, CA, June 1974. Also BRL Contract Report 149, April 1974.* (AD #920194L)

V. CONCLUSIONS

It is concluded that the technique of passively Q-switching the ruby laser can be applied profitably to photograph transient phenomena using the techniques described in this paper. Because of the high mirror rotation speeds used in these experiments (very fast film writing speed) and the fast shock wave velocities, the laser rod must be of select quality to prevent blurring of images due to overly-long pulse duration. Our success ratio was good, despite the lack of precise control of our events.

The most meaningful and accurate data were obtained when several photographs were made for a single run using the sequence laser light source; for, although the shock velocity was repeatable to ± 2% for the shadowgrams made for separate runs, scatter of the data made it difficult to draw firm conclusions.

The results suggest that: 1) the time for formation of the inner shock scales directly with the ratio of sound speed behind each shock wave for the conditions at exit, and with the ratio of tube diameters; 2) once the inner shock is complete, the outer and inner shocks have a closely spherical shape and the flow field is quasi-steady; 3) the two shocks expand from the same apparent center so that all measurements can be related to the outer shock "radius" which obeys a power law variation in time. However, it may not be appropriate to try to correlate the experimental data with blast theory for a point source, because in our case, we have a rather large source (relative to our proximity to it), which is distributed over a circular cross-section.

MJS-1 must be used to make interferograms of projectiles being launched using air as a driver gas and air as a receiver gas. MJS-2 is unsuitable, because the turbulent driver gas destroys the fringe pattern. However, MJS-2 was especially useful in obtaining shadow photographs and pressure measurements in the flow field with less manpower.

ACKNOWLEDGMENT

Messrs. Donald F. McClellan and William G. Thompson are due a special acknowledgment for their expert technical assistance and their "make it work" attitude during the course of this work.

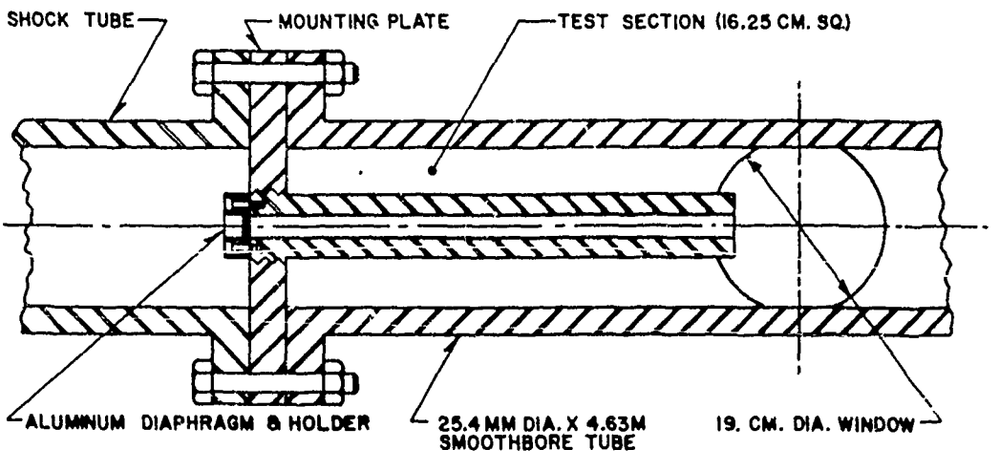

Figure 1. Cross-Section of Muzzle Jet Flow Simulator, MJS-1

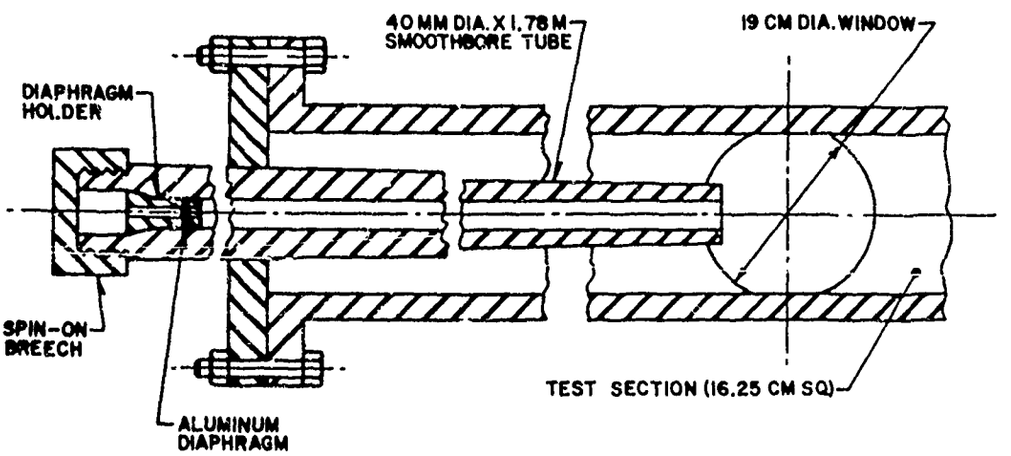

Figure 2. Cross-Section of Muzzle Jet Flow Simulator, MJS-2

Figure 3 (To the right):
Plan View of the Optical Set-up

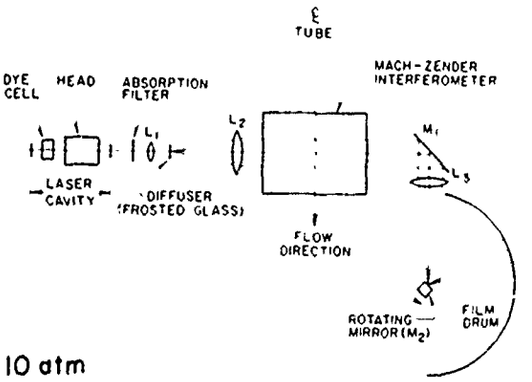

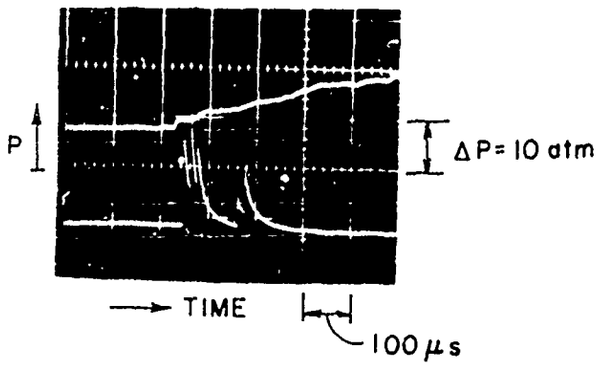

Figure 4: Simultaneously-Triggered Dual Beam Oscilloscope Traces: Static Pressure Near the Muzzle of MJS-1 (upper trace); Sequence of Laser Multiple-Pulses (lower trace).

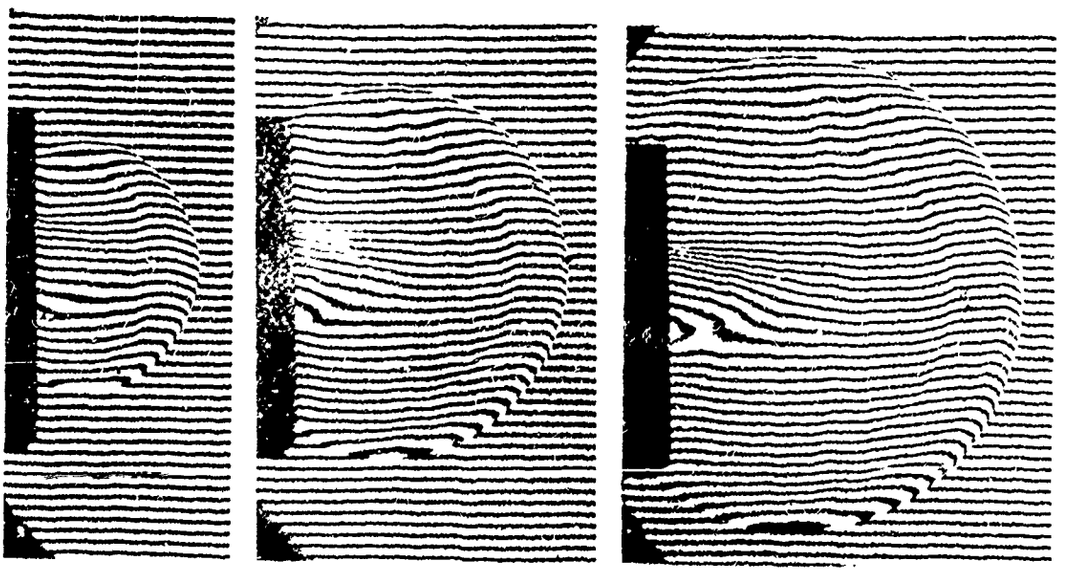

a. 20 μs b. 35 μs c. 49 μs

Figure 5: Sequence of Multiple-Pulse Laser Interferograms in MJS-1 for a Single Run in Air. λ = 6943Å; $M_{s_e} \sim 4.5$; $p_e/p_\infty \sim 75$; $M_e > 1$; Writing Speed ~ 16.2mm/μs

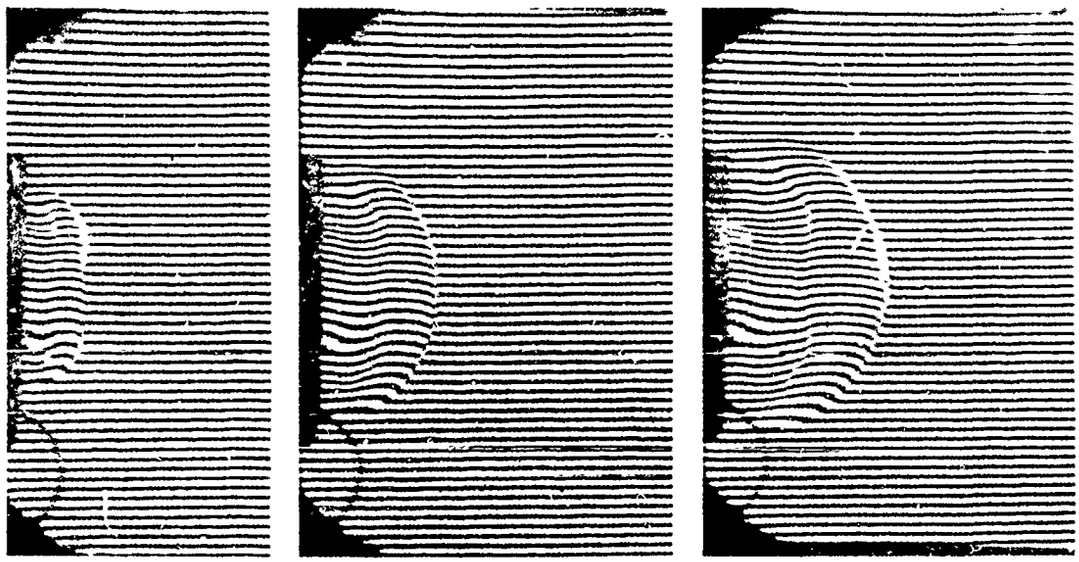

a. 18.5 μs b. 34 μs c. 49 μs

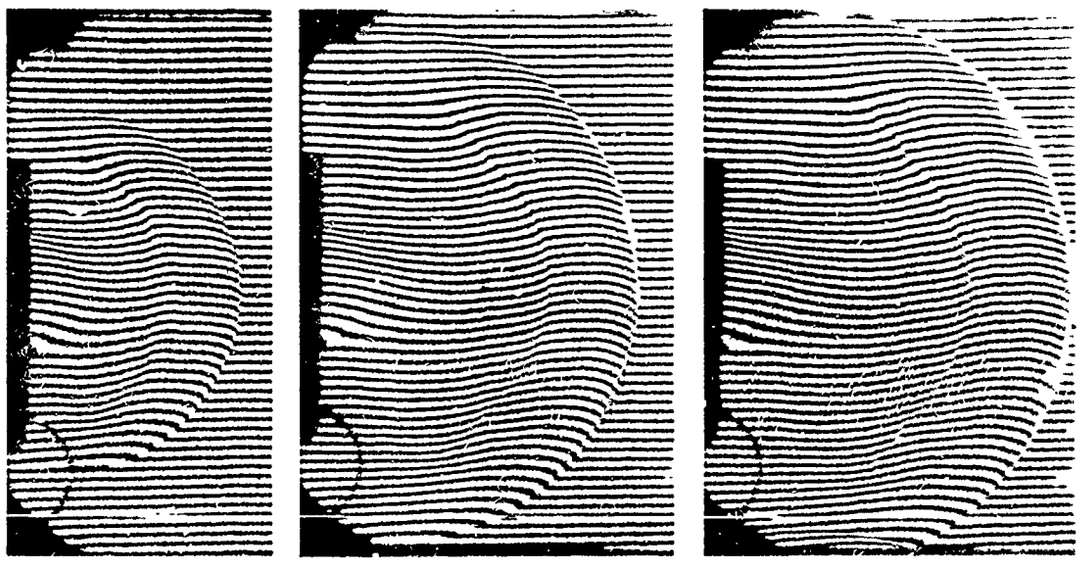

d. 67 μs e. 115 μs f. 132 μs

Figure 6: Sequence of Multiple-Pulse Laser Interferograms in MJS-2 for a Single Run in Air. λ = 6943Å; $M_{s_e} \sim 2.8$; $p_e/p_\infty \sim 7$; $M_e > 1$; Writing Speed ~ 18.6mm/μs

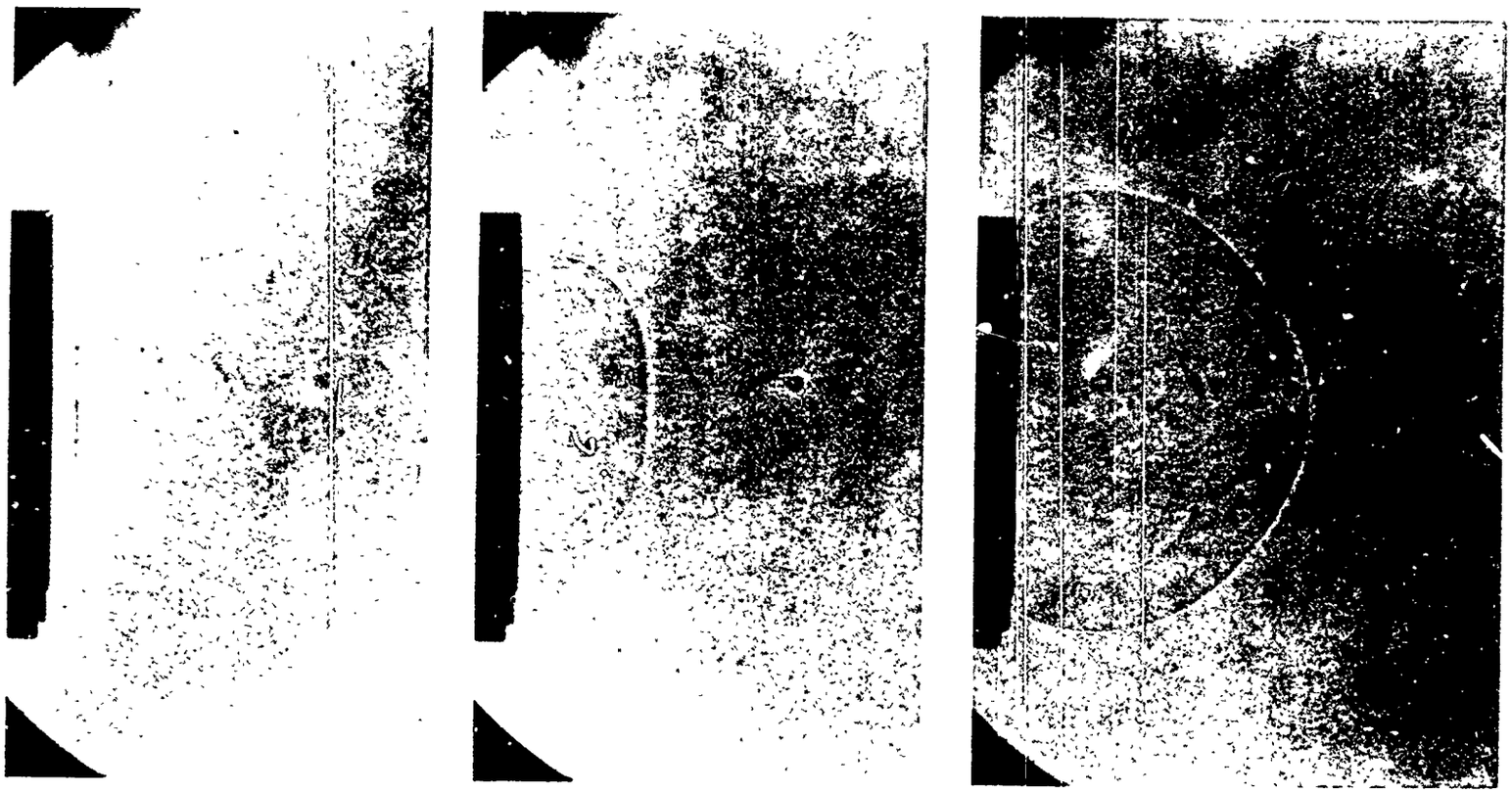

a. 3.4 μs b. 13.4 μs c. 33.3 μs

Figure 7: Series of Spark Shadow Photographs Made in MJS-2 for Separate Runs in Air. $M_{s_e} \sim 5.6$; $p_e/p_\infty \sim 30$; $M_e > 1$

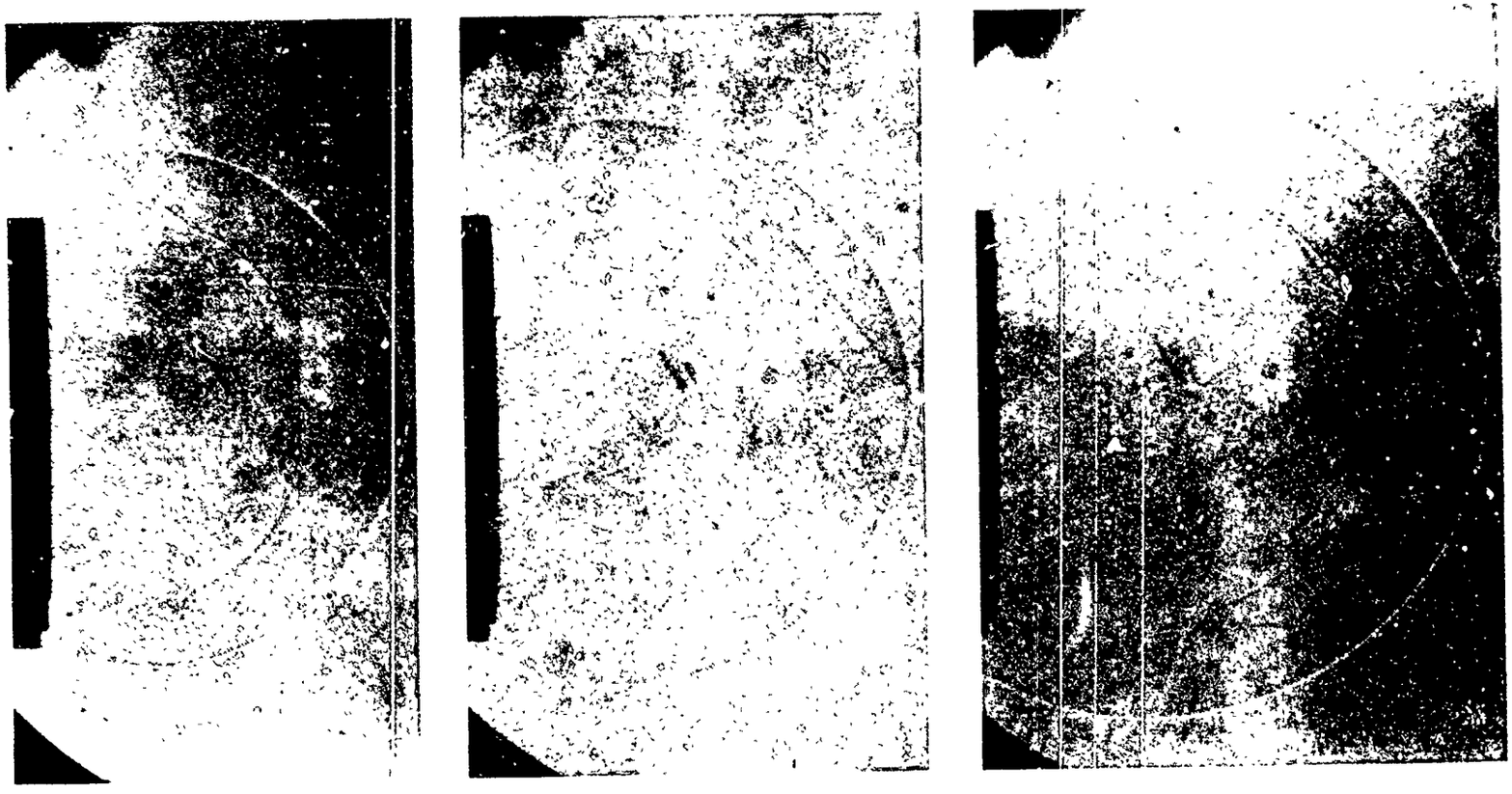

d. 43.3 μs e. 51.5 μs f. 68.7 μs

Figure 7: Series of Spark Shadow Photographs Made in MJS-2 for Separate Runs in Air. $M_{s_e} \sim 5.6$; $p_e/p_\infty \sim 30$; $M_e > 1$

a. 29 μs b. 90 μs c. 191 μs

Figure 8: Series of Spark Shadow Photographs in MJS-2 for Separate Projectile Launches in Air. Nitrogen Propelling Gas; Projectile Mass ~ 75 gm; Muzzle Velocity ~ 240 m/s; $p_e/p_\infty \sim 160$

Figure 9a: Spark Shadowgraph of Pancake Gage (see the insert) in the Flow

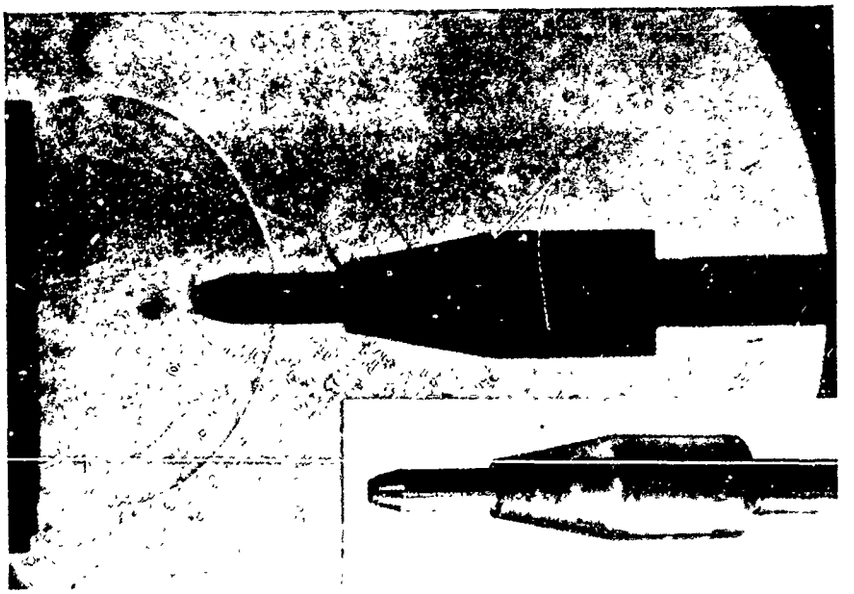

Figure 9b: Spark Shadowgraph of Pitot Pressure Gage (see the insert) in the Flow

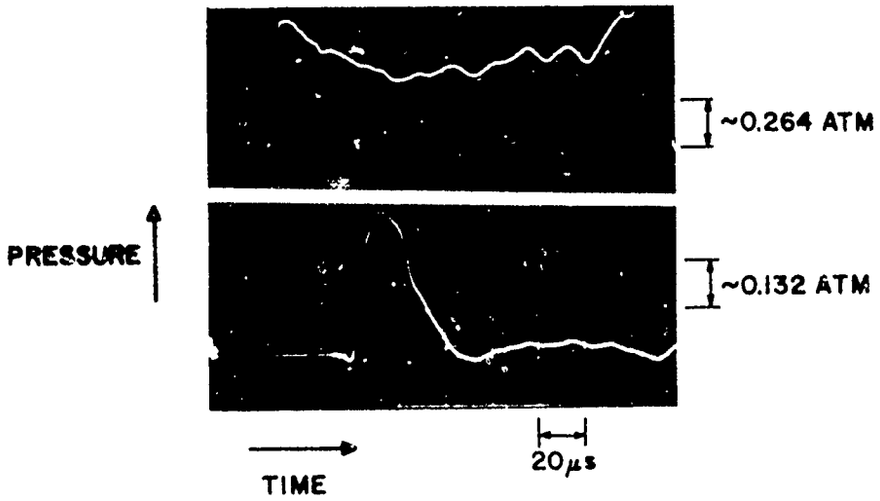

Figure 10: Oscilloscope Traces of Static Pressure Measured as in Figure 9a. Sensing Element Location from the Muzzle: ∿ 26mm (upper trace), ∿ 82mm (lower trace).

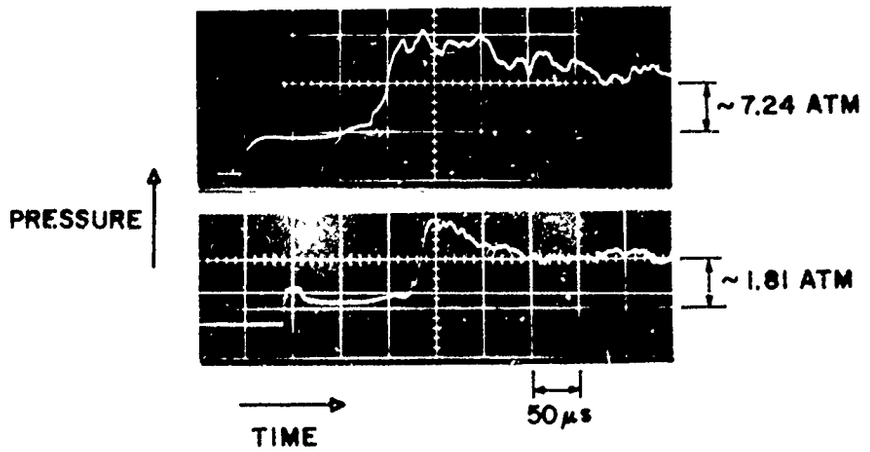

Figure 11: Oscilloscope Traces of Pitot Pressure Measured as in Figure 9b. Sensing Element Location from the Muzzle: ∿ 32mm (upper trace); ∿ 86mm (lower trace).

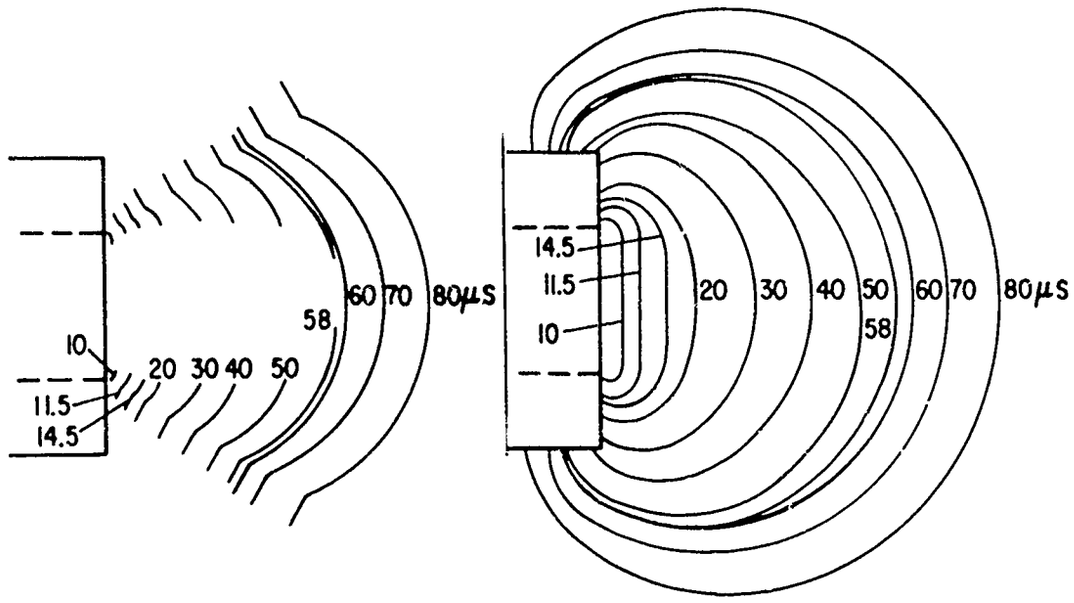

a. Inner Shock Wave. b. Outer Shock Wave

Figure 12: Contours Showing Motion of the Shock Waves in Time. Times should be reduced by ∿ 6.5 μs to be elapsed times after exit from the muzzle.

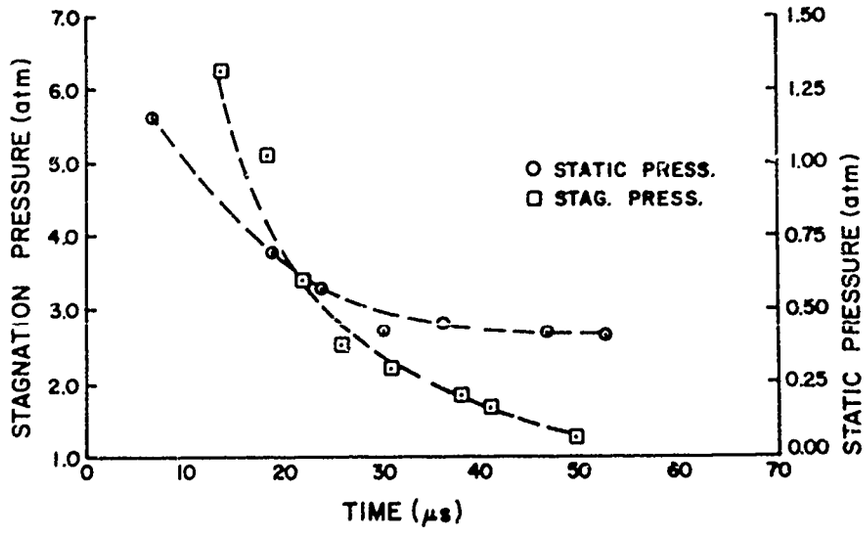

Figure 13: Peak Static Pressure and Pitot Pressure Measured Behind the Shock Wave, as in Figures 9-11. Times are the same as on Figure 12.

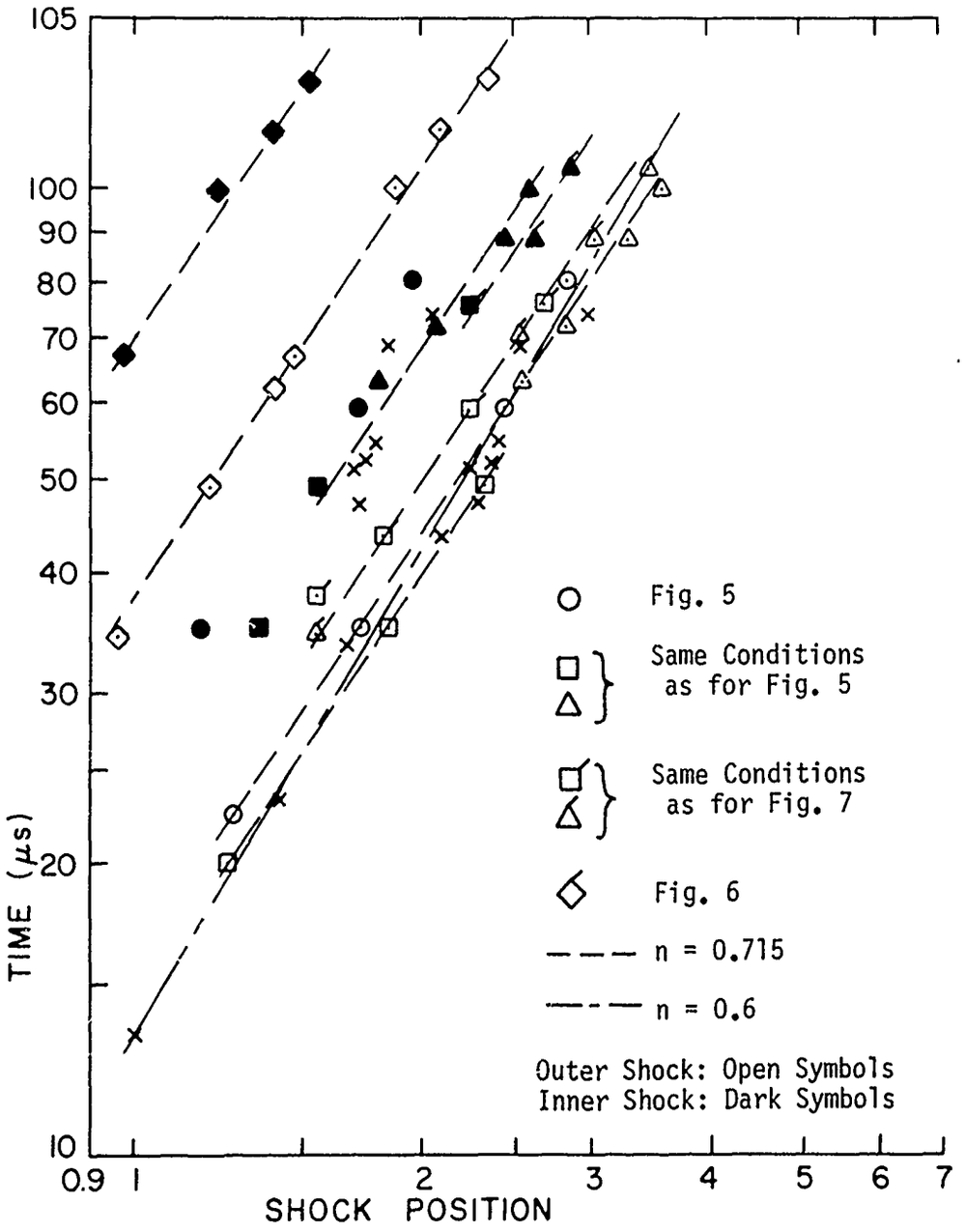

Figure 14: Inner and Outer Shock Positions on the Jet Axis as Functions of Elapsed Time After Exit from the Muzzle. Shock Position is in Multiples of Diameters of the Tube in MJS-1.

REFERENCES

1. K. Oswatitsch, "Intermediate Ballistics," Deutsche Luft und Raumfahrt Forschungs - Bericht 64-37, DVL Bericht 358, 1964.

2. C. Cranz and B. Glatzel, "Die Ausströmung von Gasen Bei Hohen Anfangsdrucken," *Ann. der Physik*, Vol. 43, 1914.

3. G. A. Schroeder, "Experimentelle Untersuchungen zur Stroemungsausbildung in der Pulvergasglocke," Bericht E4-71, Arbeitsgruppe für Ballistische Forschung, Weil am Rhein, 1971.

4. E. M. Schmidt and D. D. Shear, "The Formation and Decay of Impulsive, Supersonic Jets," AIAA Paper No. 74-531, AIAA 7th Fluid and Plasma Dynamics Conference, Palo Alto, CA, June 1974. Also BRL Report 1692, "The Flow Field About an M-16 Rifle," January 1974, AD 916646L.

5. E. M. Schmidt, "Muzzle Devices, A State-of-the-Art Survey. Volume I: Hardware Study," BRL Memo Report 2276, February 1973, AD 909325L.

6. T. C. Adamson, Jr., "The Structure of the Rocket Exhaust Plume Without Reaction at Various Altitudes," *Supersonic Flow, Chemical Processes and Radiation Transfer*, Pergamon Press, New York, 1964.

7. J. D. Buckmaster, "An Investigation of Cylindrical Starting Flows," *AIAA Journal*, Vol. 2, No. 8, September 1964.

8. I. M. Naboko, T. V. Bazhenova, A. I. Opera, and V. A. Belavin, "Formation of a Jet of Shock-Heated Gas Outflowing into Evacuated Space." *Astronautica Acta*, Vol. 17, Pergamon Press, New York, 1972.

9. C. K. Zoltani, "Evaluation of the Computer Codes BLAST DORF, HELP, and HEMP for Suitability of Underexpanded Jet Flow Calculation," BRL Report 1659, August 1973, AD 768708.

10. F. H. Oertel, Jr., "Laser Interferometry of Unsteady, Underexpanded Jets," Proc. Int'l. Cong. Instr. in Aerospace Simulation Facilities, California Institute of Technology, Pasadena, CA, 1973. Also BRL Report 1694, January 1974, AD 773664.

11. I. I. Glass and J. G. Hall, *Handbook of Supersonic Aerodynamics, Shock Tubes, Section 18*, NAVORD Report 1488 (Vol. 6), 1959.

12. H. Schlichting, *Boundary Layer Theory*, McGraw-Hill Book Company, Inc., New York, 1960.

REFERENCES (Continued)

13. R. L. Rowe, "Interferometers for Hypervelocity Ranges," *ISA Trans.*, Vol 5, No. 1, 1966.

14. P. S. Westine and F. Hoese, "Blast Gauge for Measuring Shocks with Short Wavelengths," Southwest Research Institute Interim Report, Contract No. 0178-69-C-0318, May 1970.

15. R. Ladenburg, C. C. Van Voorhis, and J. Winckler, "Interferometric Studies of Faster than Sound Phenomena, Part II. Analysis of Supersonic Air Jets," *Phys. Rev.*, Vol. 76, No. 5, 1949.

16. F. D. Bennett, W. C. Carter, and V. E. Bergdolt, "Interferometric Analysis of Air Flow About Projectiles in Free Flight," *J. Appl. Phys.*, Vol. 23, No. 4, 1952; also BRL Report No. 797, March 1952, AD 801758.

17. A. K. Celmins, "Theoretical Basis of the Recoiless Rifle Interior Ballistics Code RECRIF," BRL Report (to be published).

18. J. I. Erdos and P. D. Del Guidice, "Gas Dynamics of Muzzle Blast," AIAA Paper No. 74-532, AIAA 7th Fluid and Plasma Dynamics Conference, Palo Alto, CA, June 1974. Also BRL Contract Report 149, April 1974. (AD #920194L)

LIST OF SYMBOLS

a	local sound speed
L_1, L_2, L_3	lenses on Figure 3
$M = u/a$	Mach No. of gas behind the shock wave
$M_s = U_s/a_\infty$	Mach No. of the shock wave
M_1, M_2	mirrors on Figure 3
p	pressure
t	time
X	distance measured from the muzzle
λ	wavelength of observing light
η	power law exponent
Subscripts	
c	denotes apparent center of expanding shock wave
e	conditions at muzzle exit
i	denotes inner shock wave
o	denotes outer shock wave
∞	conditions in ambient gas

DISTRIBUTION LIST

No. of Copies	Organization
2	Commander Defense Documentation Center ATTN: DDC-TCA Cameron Station Alexandria, VA 22314
1	Director Defense Nuclear Agency Washington, DC 20305
1	Commander US Army Materiel Development and Readiness Command ATTN: DRCDMA-ST 5001 Eisenhower Avenue Alexandria, VA 22333
1	Commander US Army Aviation Systems Command ATTN: DRSAV-E 12th and Spruce Streets St. Louis, MO 63166
1	Director US Army Air Mobility Research and Development Laboratory Ames Research Center Moffett Field, CA 94035
1	Commander US Army Electronics Command ATTN: DRSEL-RD Fort Monmouth, NJ 07703
1	Commander US Army Missile Command ATTN: DRSMI-R Redstone Arsenal, AL 35809
5	Commander US Army Missile Command ATTN: DRSMI-RDK Mr. R. Becht (4 cys) Mr. R. Deep Redstone Arsenal, AL 35809
1	Commander US Army Tank Automotive Development Command ATTN: DRDTA-RWL Warren, MI 48090
2	Commander US Army Mobility Equipment Research & Development Command ATTN: Tech Docu Cen, Bldg. 315 DRSME-RZT Fort Belvoir, VA 22060
3	Commander US Army Armament Command ATTN: P. Ehle E. Haug Tech Lib Rock Island, IL 61202
2	Commander US Army Armament Command ATTN: Rodman Laboratories S. Thompson S. Burley Rock Island, IL 61202
6	Commander US Army Frankford Arsenal ATTN: Mr. T. Boldt SARFA-U2100 Mr. J. Mitchell SARFA-U3100, S.Fulton SARFA-U3300 Mr. S. Hirshman Mr. A. Cianciosi L4100-150-2 Mr. C. Sleischer, Jr. Philadelphia, PA 19137
4	Commander US Army Picatinny Arsenal ATTN: SARPA-DR-D, S. Wasserman SARPA-DR-V, Mr. A. Loeb Mr. D. Mertz Mr. E. Friedman Dover, NJ 07801

DISTRIBUTION LIST

No. of Copies	Organization
5	Commander US Army Picatinny Arsenal ATTN: SARPA-V, E. Walbrecht Mr. S. Verner SARPA-VE, Dr. Kaufman SARPA-FR-M-MA Mr. E. Barrieres SARPA-D, Mr. Lindner Dover, NJ 07801
2	Commander US Army Watervliet Arsenal ATTN: Tech Lib SARWV-PDR-S, F. Sautter Watervliet, NY 12189
1	Commander US Army Harry Diamond Labs ATTN: DRXDO-TI 2800 Powder Mill Road Adelphi, MD 20783
1	Director US Army TRADOC Systems Analysis Activity ATTN: ATAA-SA White Sands Missile Range NM 88002
1	Commander US Army Materials and Mechanics Research Center ATTN: DRXMR-ATL Watertown, MA 02172
1	Commander US Army Natick Research and Development Center ATTN: DRXRE, Dr. D. Sieling Natick, MA 01762
1	Commander US Army Research Office ATTN: CRD-AA-EH P. O. Box 12211 Research Triangle Park, NC 27709
1	Commander US Army Ballistic Missile Defense Systems Command Huntsville, AL 35804
1	Director US Army Advanced BMD Technology Center P. O. Box 1500, West Station Huntsville, AL 35809
3	Commander US Naval Air Systems Command ATTN: AIR-604 Washington, DC 20360
3	Commander US Naval Ordnance Systems Command ATTN: ORD-9132 Washington, DC 20360
2	Commander and Director David W. Taylor Naval Ship Research & Development Center ATTN: Tech Lib Aerodynamic Lab Bethesda, MD 20084
3	Commander US Naval Surface Weapons Center ATTN: Code 312, F. Regan Mr. S. Hastings Code 730, Tech Lib Silver Spring, MD 20910
3	Commander US Naval Surface Weapons Center ATTN: Code GX, Dr. W. Kemper Mr. F. H. Maille Dr. G. Moore Dahlgren, VA 22448
1	Commander US Naval Weapons Center ATTN: Code 553, Tech Lib China Lake, CA 93555

DISTRIBUTION LIST

No. of Copies	Organization
3	Director US Naval Research Laboratory ATTN: Tech Info Div Code 7700, D. A. Kolb Code 7720, Dr.E.McClean Washington, DC 20390
1	Commander US Naval Ordnance Station ATTN: Code FS13A, P. Sewell Indian Head, MD 20640
2	ADTC (ADBPS-12) Eglin AFB, FL 32542
1	AFATL (DLDG) Eglin AFB, FL 32542
1	AFATL (DLY) Eglin AFB, FL 32542
2	AFATL (DLDL, Dr. D.C. Daniel) Eglin AFB, FL 32542
1	AFWL (DEV) Kirtland AFB, NM 87117
1	ASD (ASBEE) Wright-Patterson AFB, OH 45433
1	Director NASA Scientific and Technical Information Facility ATTN: SAK/DL P. O. Box 8757 Baltimore/Washington International Airport, MD 21240
1	Director Jet Propulsion Laboratory ATTN: Tech Lib 2800 Oak Grove Drive Pasadena, CA 91103
2	Director National Aeronautics and Space Administration George C. Marshall Space Flight Center ATTN: MS-I, Lib R-AERO-AE, A. Felix Huntsville, AL 35812
1	Director National Aeronautics and Space Administration Langley Research Center ATTN: MS 185, Tech Lib Langley Station Hampton, VA 23365
1	Advanced Technology Labs ATTN: Dr. J. Erdos Merrick & Stewart Avenues Westbury, NY 11590
2	ARO, Inc ATTN: Tech Lib Arnold AFS, TN 37389
1	Technical Director Colt Firearms Corporation 150 Huyshore Avenue Hartford, CT 14061
1	General Electric Corporation Armaments Division ATTN: Mr. R. Whyte Lakeside Avenue Burlington, VT 05401
1	Northrop Corporation Aircraft Division ATTN: Dr. A. Wortman 3901 W. Broadway Hawthorne, CA 90250

DISTRIBUTION LIST

No. of Copies	Organization
1	Winchester Western Division Olin Corporation ATTN: Mr. D. Merrill New Haven, CT 06504
1	Sandia Laboratories ATTN: Aerodynamics Dept Org 5620, R. Maydew P. O. Box 5800 Albuquerque, NM 87115
1	Guggenheim Aeronautical Lab California Institute of Technology ATTN: Tech Lib Pasadena, CA 91104
1	Calspan Corporation ATTN: Mr. G. A. Sterbutzel P. O. Box 235 Buffalo, NY 14221
2	Franklin Institute ATTN: Dr. Carfagno Dr. Wachtell Race & 20th Streets Philadelphia, PA 19103
1	The Johns Hopkins University Applied Physics Laboratory Johns Hopkins Road Laurel, MD 20810
1	The Johns Hopkins University ATTN: Dr. F. D. Bennett Dept of Mechanics and Material Sciences 34th and Charles Streets Baltimore, MD 21218
1	Massachusetts Institute of Technology Department of Aeronautics and Astronautics ATTN: Tech Lib 77 Massachusetts Avenue Cambridge, MA 02139
1	Ohio State University Department of Aeronautics and Astronautical Engineering ATTN: Tech Lib Columbus, OH 43210
1	Polytechnic Institute of Brooklyn Graduate Center ATTN: Tech Lib Farmingdale, NY 11735
1	Director Forrestal Research Center Princeton University Princeton, NJ 08540
1	Forrestal Campus Library Princeton University P. O. Box 710 Princeton, NJ 08540
1	Southwest Research Institute ATTN: Mr. Peter S. Westine P. O. Drawre 28510 8500 Culebra Road San Antonio, TX 78228
	Aberdeen Proving Ground Marine Corps Ln Ofc Dir, USAMSAA